

Sub-stochiometric MoO_x by radio-frequency magnetron sputtering as hole-selective passivating contacts for silicon heterojunction solar cells

Xiufang Yang(杨秀芳), Shengsheng Zhao(赵生盛), Qian Huang(黄茜), Cao Yu(郁超), Jiakai Zhou(周佳凯), Xiaoning Liu(柳晓宁), Xianglin Su(苏祥林), Ying Zhao(赵颖), and Guofu Hou(侯国付)

Citation: Chin. Phys. B, 2022, 31 (**9**): 098401. DOI: 10.1088/1674-1056/ac5a42
Journal homepage: http://cpb.iphy.ac.cn; http://iopscience.iop.org/cpb

What follows is a list of articles you may be interested in

Applications and functions of rare-earth ions in perovskite solar cells

Limin Cang(苍利民), Zongyao Qian(钱宗耀), Jinpei Wang(王金培), Libao Chen(陈利豹), Zhigang Wan(万志刚), Ke Yang(杨柯), Hui Zhang(张辉), and Yonghua Chen(陈永华)

Chin. Phys. B, 2022, 31 (**3**): 038402. DOI: 10.1088/1674-1056/ac373a

Theoretical investigation of halide perovskites for solar cell and optoelectronic applications

Jingxiu Yang(杨竞秀), Peng Zhang(张鹏), Jianping Wang(王建平), and Su-Huai Wei(魏苏淮)†

Chin. Phys. B, 2020, 29 (**10**): 108401. DOI: 10.1088/1674-1056/abb3f6

SiO_2 nanoparticle-regulated crystallization of lead halide perovskite and improved efficiency of carbon-electrode-based low-temperature planar perovskite solar cells

Zerong Liang(梁泽荣), Bingchu Yang(杨兵初), Anyi Mei(梅安意), Siyuan Lin(林思远), Hongwei Han(韩宏伟), Yongbo Yuan(袁永波), Haipeng Xie(谢海鹏), Yongli Gao(高永立), Conghua Zhou(周聪华)

Chin. Phys. B, 2020, 29 (**7**): 078401. DOI: 10.1088/1674-1056/ab8da5

Photocurrent improvement of an ultra-thin silicon solar cell using the localized surface plasmonic effect of clustering nanoparticles

F Sobhani, H Heidarzadeh, H Bahador

Chin. Phys. B, 2020, 29 (**6**): 068401. DOI: 10.1088/1674-1056/ab836d

Improving power conversion efficiency of perovskite solar cells by cooperative LSPR of gold-silver dual nanoparticles

Peng Liu(刘鹏), Bing-chu Yang(杨兵初), Gang Liu(刘钢), Run-sheng Wu(吴闰生), Chu-jun Zhang(张楚俊), Fang Wan(万方), Shui-gen Li(李水根), Jun-liang Yang(阳军亮), Yong-li Gao(高永立), Cong-hua Zhou(周聪华)

Chin. Phys. B, 2017, 26 (**5**): 058401. DOI: 10.1088/1674-1056/26/5/058401

Sub-stochiometric MoO_x by radio-frequency magnetron sputtering as hole-selective passivating contacts for silicon heterojunction solar cells

Xiufang Yang(杨秀芳)[1,2,3,4], Shengsheng Zhao(赵生盛)[1,2,3,4], Qian Huang(黄茜)[1,2,3,4,‡], Cao Yu(郁超)[5], Jiakai Zhou(周佳凯)[1,2,3,4], Xiaoning Liu(柳晓宁)[1,2,3,4], Xianglin Su(苏祥林)[1,2,3,4], Ying Zhao(赵颖)[1,2,3,4], and Guofu Hou(侯国付)[1,2,3,4,†]

[1] *Institute of Photoelectronic Thin Film Devices and Technology of Nankai University, Tianjin* 300350, *China*
[2] *Key Laboratory of Photoelectronic Thin Film Devices and Technology of Tianjin, Tianjin* 300350, *China*
[3] *Collaborative Innovation Center of Chemical Science and Engineering (Tianjin), Tianjin* 300072, *China*
[4] *Engineering Center of Thin Film Photoelectronic Technology of Ministry of Education, Tianjin* 300350, *China*
[5] *Suzhou Maxwell Automation Equipment Co. Ltd, Suzhou* 215299, *China*

(Received 13 January 2022; revised manuscript received 2 March 2022; accepted manuscript online 3 March 2022)

The silicon heterojunction (SHJ) solar cell has long been considered as one of the most promising candidates for the next-generation PV market. Transition metal oxides (TMOs) show good carrier selectivity when combined with c-Si solar cells. This has led to the rapid demonstration of the remarkable potential of TMOs (especially MoO_x) with high work function to replace the p-type a-Si:H emitting layer. MoO_x can induce a strong inversion layer on the interface of n-type c-Si, which is beneficial to the extraction and conduction of holes. In this paper, the radio-frequency (RF) magnetron sputtering is used to deposit MoO_x films. The optical, electrical and structural properties of MoO_x films are measured and analyzed, with focus on the inherent compositions and work function. Then the MoO_x films are applied into SHJ solar cells. When the MoO_x works as a buffer layer between ITO/p-a-Si:H interface in the reference SHJ solar cell, a conversion efficiency of 19.1% can be obtained. When the MoO_x is used as a hole transport layer (HTL), the device indicates a desirable conversion efficiency of 17.5%. To the best of our knowledge, this current efficiency is the highest one for the MoO_x film as HTL by RF sputtering.

Keywords: radio-frequency magnetron sputtering, silicon heterojunction (SHJ) solar cell, MoO_x, hole transport layer

PACS: 84.60.Jt, 88.40.H–, 88.40.jj **DOI:** 10.1088/1674-1056/ac5a42

1. Introduction

In the past decades, amorphous/crystalline silicon heterojunction solar cells have been one of the most promising candidates for low-cost and highly-efficient solar cells.[1,2] Intrinsically hydrogenated amorphous silicon (a-Si:H(i)) films have been widely adopted as the passivating layer and emitting layer in the silicon heterojunction (SHJ) solar cells, which effectively enhance the open circuit voltage (V_{oc}). Kaneka Co. Ltd has reported heterojunction interdigitated back contact (HJ-IBC) cell with the record efficiency of 26.63%.[3] However, the unavoidable parasitic absorption caused by a-Si:H passivating layer and emitting layer is considered as the main limitation to further improve the SHJ device performance. In order to get p-type or n-type a-Si:H layers, highly toxic PH_3 or B_2H_6 dopants are usually adopted. In addition, the heavily doped carrier selective layer (n^+, p^+) leads to serious carrier combination. Therefore, hydrogenated amorphous silicon alloyed with carbon, oxygen and nitrogen etc. are used to obtain wide bandgap silicon films to partially decrease the parasitic absorption.[4–6] Many researchers have tried to adjust the work function of the n^+/p^+ layers by optimizing doping techniques to achieve better band matching effects with c-Si.[7–9] Other studies have proven that it is a more convenient and effective way to insert a buffer layer with high work function to further extract carriers at the c-Si interface.[10–14]

Recently, novel carrier-selective passivating materials have been extensively developed, especially non-stoichiometric transition metal oxides with high work function including WO_x ($x < 3$),[7] V_2O_x ($x < 5$),[15,16] CrO_x ($x < 3$)[17,18] and MoO_x ($x < 3$).[7,19–21] Among them, MoO_x has attracted extensive attention as a hole selective transport layer (HTL) in organic solar cells and undoped asymmetric heterogeneous contact (DASH) silicon solar cells due to its high work function and unique electrical and optical properties.[21–25] The combination of high work function MoO_x with lightly doped c-Si(n) substrate will lead to upward band bending at the c-Si interface, and the Fermi level of MoO_x close to the valence band of c-Si absorber, forming a favorable level alignment for band to band (B2B) hole transport.[26–28]

Various deposition techniques such as thermal

†Corresponding author. E-mail: gfhou@nankai.edu.cn
‡Corresponding author. E-mail: carolinehq@nankai.edu.cn

© 2022 Chinese Physical Society and IOP Publishing Ltd

evaporation,[29] electron beam evaporation,[30] pulsed laser deposition,[31] and sputtering[32–35] and sol-gel process[36] were employed for the growth of MoO_x films. Compared with the traditional coating technology, magnetron sputtered films have stronger adhesion with the substrate, and it is more convenient to fabricate the films with high melting point materials. It is easy to control the composition of the films by varying the target material and to realize reactive sputtering, which can be more convenient for plating a variety of films. RF sputtered is preferred to other deposition methods for large area and good reproducibility, too. Recently, several groups reported MoO_x films by reactive sputtering from the Mo metal target and applying MoO_x films as hole-selective contacts in SHJ cells. Boccard *et al.* observed a barrier for hole extraction due to the stoichiometric issues. It has been demonstrated that TMOs thin films with low average oxidation state present better transport properties, while moderate carrier selectivity.[37] Bivour *et al.* demonstrated the suitability of sputtered MoO_x thin film as a carrier-selective contact for the n-type silicon (n-Si) wafer, and highlighted the importance of higher work function MoO_x film to improve the hole-selectivity due to c-Si upward band bending at the n-Si/MoO_x interface.[38] So far, several groups have reported MoO_x-based SHJ solar cells with efficiencies up to 22% or even the highest one of 23.5%.[39] In most cases the evaporation method is adopted to deposit MoO_x films. Truth to be told that the evaporation is not a popular method in industrial production, at least not as good as the sputtering one. It is worth mentioning that sputtered MoO_x films as HTL for c-Si SHJ solar cell has not been reported with efficiency over than 15% up to now.

In this experiment, we demonstrated magnetron sputtered MoO_x films and applications in SHJ solar cells. The results show that the MoO_x film as a buffer layer effectively improve the SHJ device efficiency to 19.1%. Meanwhile, we demonstrated that MoO_x can replace p-type a-Si:H emitting layer as a hole selective transport layer, resulting in a conversion efficiency of 17.5 %, which is the highest one for the MoO_x film as HTL by RF sputtering, to the best of our knowledge.

2. Experimental details

2.1. Film and device fabrication

All the solar cells were fabricated on CZ n-type c-Si (5 cm×5 cm, 1–3 Ω, 180 μm) substrates. A stack composed of a-Si:H(i)/a-Si:H(n or p) was deposited at the both sides by plasma enhanced chemical vapor deposition (PECVD) at 300 °C on all substrates. The MoO_x films were deposited on n-type c-Si and Eagle glass substrates by 13.56 MHz RF magnetron sputtering from a MoO_3 (> 99.95%) target. MoO_x sputtering process was done in a vacuum chamber (base pressure before deposition $\sim 2\times10^{-4}$ Pa), from a stoichiometric MoO_3 target at 160 °C, with argon flow of 60 sccm, working pressure at 2×10^{-4} Pa and RF power density with 1.75 W/cm^2. In order to ensure the same experimental conditions, the target was pre-sputtered in argon for about 30 minutes before the formal deposition. Then, ITO films with thickness about 80–100 nm were prepared on passivated selective contacts by using thermal evaporated method. Finally, 800 nm thick Ag+Al gridlines were deposited on the front surface by using thermal evaporated, and Al electrodes of the same thickness were deposited on the rear field. In our work, the performances of solar cells with MoO_x film as buffer layer and HTL are analyzed, respectively. The schematic structures of fabricated solar cells are shown in Fig. 1. During the test, a reticle was used to block the redundant part, and the illumination area was 1 cm×1 cm.

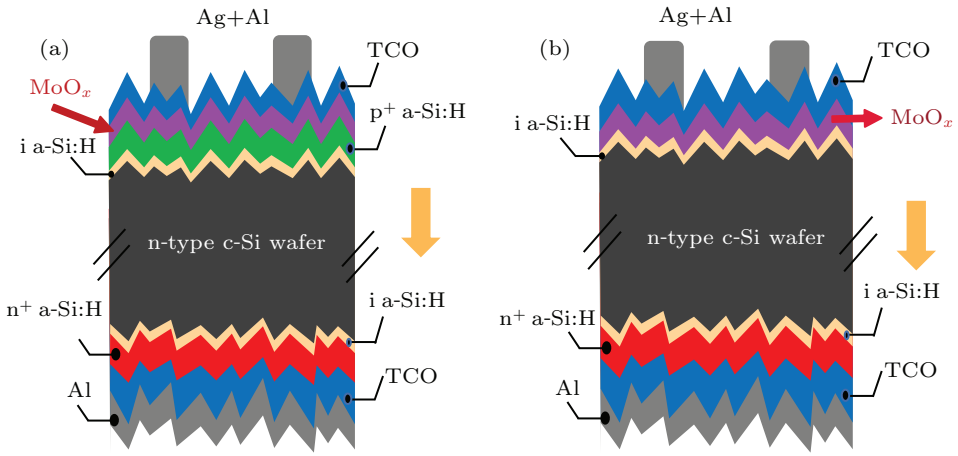


Fig. 1. Schematic structures of SHJ solar cells with MoO_x as buffer layer (a) and hole transport layer (b), respectively.

2.2. Film and device characteristics

Top-view of scanning electron microscopy (SEM) images were characterized by Jeol JSM-6700F scanning electron microscope. The quasi-steady state photoconductivity decay (QSSPC) method was used to measure the minority carrier lifetime of the samples by the WCT-120 minority carrier life-

time tester from Sinton Instruments company. The x-ray photoelectron spectroscopy (XPS) and ultraviolet photoelectron spectroscopy (UPS) measurements of the MoO_x films coated on indium tin oxides (ITO) were performed in an ESCALAB 250Xi. Finally, the solar cells were tested with a Wacom solar simulator (WXS-156S-L2, AM1.5GMM) under the room temperature of 25 °C, standard spectrum AM1.5 and power density of 100 mW/cm^2. The quantum efficiency of the devices was tested by the QEX10 quantum efficiency system from PV Measurements company.

3. Results and discussion

3.1. Surface morphology of MoO_x film

The MoO_x films were prepared by magnetron sputtering process of specific target and deposited on a-Si:H(i)/c-Si with film thickness of 5 nm and 30 nm, respectively. Morphology of MoO_x films is a crucial factor to affect the performance of as-fabricated devices. The SEM images of MoO_x films reveal uniform and dense surface morphologies, where no obvious cracks can be observed for the sample, indicating the positive effect on the devices (Figs. 2(a) and 2(b)). Moreover, it can be seen that an ultrathin MoO_x film can fully cover the pyramidally textured surface. Fortunately, no cracks appeared at the bottoms of the pyramids when the MoO_x film thickness increased to 30 nm.

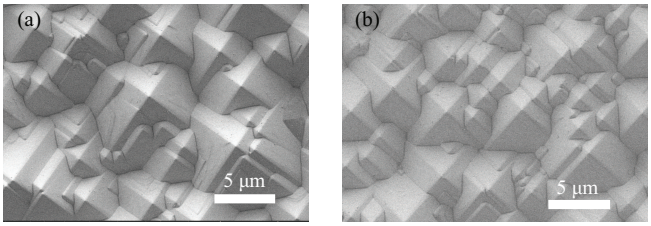


Fig. 2. SEM images of (a) 5 nm MoO_x and (b) 30 nm MoO_x films. All scale bars are 5 μm.

3.2. The passivation quality of sputtered MoO_x layer

As we all know, sputtered damage is inevitable in the thin film fabrication process. When the precursors migrate through the deposition chamber and reach the c-Si substrate, the sputtered particle groups or atoms from the target usually have enough energy to damage passivation layer. Therefore, this has prompted scientists to develop new techniques to circumvent the bombardment on passivation layer during sputtering process. Studies have shown that environmental annealing can effectively change the stoichiometric ratio of Mo/O ratio and reduce the defect density states in MoO_x films.[24] For samples subjected to ion bombardment, annealing is an effective way to restore the passivation quality. In general, the minority carrier lifetime was used to characterize the passivation performance. Minority carrier lifetime as a function of minority carrier density of samples without MoO_x, with as-sputtered 5 nm MoO_x and with post-annealed 5 nm MoO_x were measured and the results are shown in Fig. 3. For the sample with only 5 nm a-Si:H(i) passivating layer, the minority carrier lifetime is as high as 3911 μs at minority carrier density of 1×10^{15} cm^{-3} and implied open circuit voltage (iV_{oc}) of 725 mV. Then 5 nm MoO_x were subsequently sputtered, which dramatically decrease the minority carrier lifetime to 2119 μs and iV_{oc} of 710 mV. The following post-annealing with temperature of 200 °C and process duration of 60 min was performed on the sample, the minority carrier lifetime was 3752 μs and iV_{oc} of 721 mV, which is nearly as good as the original one. Since the thermal annealing can almost totally recover the passivation quality, the above results demonstrate the feasibility of application of sputtered MoO_x into SHJ solar cells to a large extent.

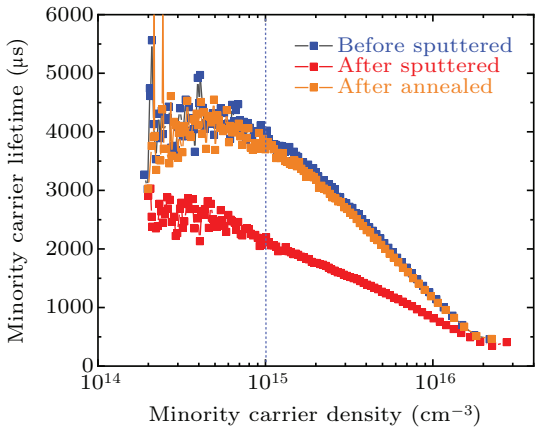


Fig. 3. Minority carrier lifetime as a function of minority carrier density of samples without MoO_x, with as-sputtered 5 nm MoO_x and with post-annealed 5 nm MoO_x.

3.3. The characteristics of MoO_x films

Affected by the preparation method and deposition conditions, the as-deposited transition metal oxide film is usually non-stoichiometric. The chemical state, element composition and electronic properties determine the work function of the transition metal oxides. Furthermore, the energy level matching of each functional layer is an important prerequisite to get better device performance. XPS was used to analyze the as-sputtered and post-annealed MoO_x films. The corresponding Mo 3d and O 1s XPS spectra are shown in Fig. 4, while the composition and binding energy positions of the oxidation state are listed in Table 1. As we all know that even if a fully stoichiometric MoO_3 target is adopted, it is still impossible to get fully stoichiometric MoO_3 films by the sputtering process. Usually, MoO_x films were obtained with x in the range from two to three, which mean that both Mo^{6+} and Mo^{5+} oxidation states exist in the films. For the as-sputtered MoO_x film in our experiments, the O/Mo ratio was calculated to be ~ 2.83. The deconvolution of the spectra was calibrated by referencing to the well-known adventitious hydrocarbon C 1s peak at

$\sim$ 284.8 eV. The spectra of Mo 3d core level energy was deconvoluted into two shoulders positioned at $\sim$ 232.6 eV and $\sim$ 231.1 eV, which correspond to Mo^{6+} and Mo^{5+} oxidation state with the Mo 3d 5/2 peak, respectively (Fig. 4(a)). Similarly, another doublet splitting represents the Mo^{6+} oxidation state with the Mo 3d 3/2 peak centered at $\sim$ 235.8 eV and the Mo^{5+} oxidation state with the Mo 3d 3/2 at $\sim$ 234.5 eV. For the post-annealed MoO_x film (Fig. 4(b)), the annealing process results with increased oxygen concentration in the film, were also revealed in the O 1s XPS (Figs. 4(c) and 4(d)). The Mo 3d curve consists of two sub-curves centered at $\sim$ 232.9 eV and at $\sim$ 231.8 eV, which represent the Mo^{6+} and Mo^{5+} oxidation state with the Mo 3d 5/2, respectively. On the contrary, shoulders peaked at $\sim$ 236.0 eV and at $\sim$ 234.9 eV represent the Mo^{6+} and Mo^{5+} oxidation state with the Mo 3d 3/2, respectively. ($\Delta_{\text{B.E.}} = E_{(\text{Mo3d3/2})} - E_{(\text{Mo3d5/2})} = 3.15$ eV).

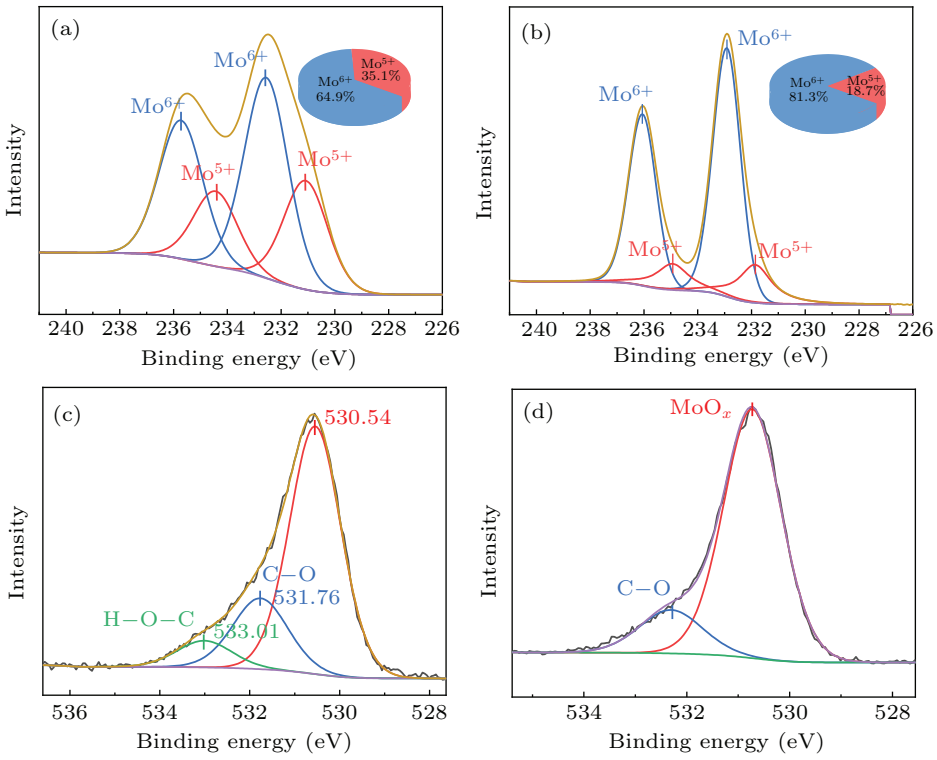


Fig. 4. XPS analysis of as-sputtered and annealed MoO_x films: (a) as-sputtered Mo 3d, (b) annealed Mo 3d, (c) as-sputtered O 1s, (d) annealed O 1s, respectively.

Table 1. Peak positions of the XPS spectra of as-sputtered and annealed MoO_x films.

Sample	Peak assignment	Binding energy (eV)	Area ratio	Element ratio
As sputtered	Mo^{6+}	$Mo3d_{5/2}$: 232.6 $Mo3d_{3/2}$: 235.8	3:2	1.85
	Mo^{5+}	$Mo3d_{5/2}$: 231.1 $Mo3d_{3/2}$: 234.5	3:2	
As-annealed	Mo^{6+}	$Mo3d_{5/2}$: 232.9 $Mo3d_{3/2}$: 236.0	3:2	4.35
	Mo^{5+}	$Mo3d_{5/2}$: 231.8 $Mo3d_{3/2}$: 234.9	3:2	

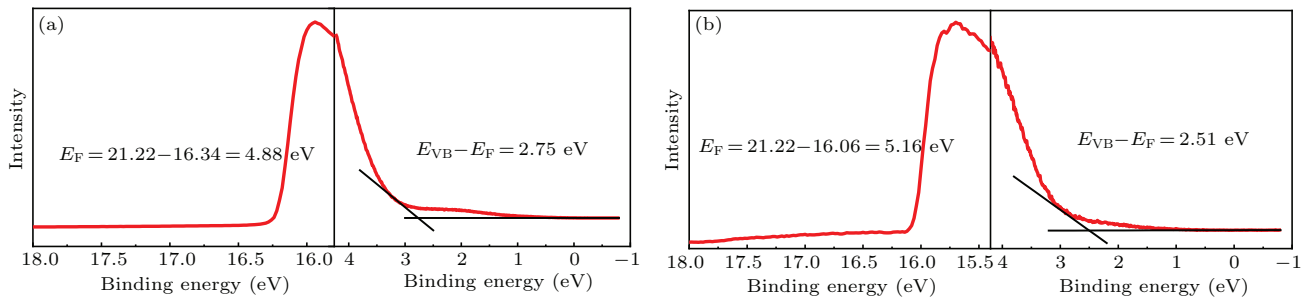


Fig. 5. UPS analysis of (a) the as-sputtered MoO_x film and (b) the post-annealed MoO_x film.

To further confirm the influence of the annealed atmosphere on the work function and oxygen vacancies of the MoO_x films, UPS measurements were performed for the corresponding films, as shown in Fig. 5. Similar to the XPS results, the UPS spectra showed an increase of the oxygen concentration in the film during annealing process. The as-sputtered MoO_x sample demonstrated a work function of 4.88 eV, while the work function of the post-annealed MoO_x increased to a much higher value of 5.16 eV, which was also much higher than that of transparent conductive oxide (TCO) (4.7 eV).[26] From the above-mentioned XPS and UPS results, the post-annealing process proved to be an effective method to control the oxygen vacancies and the existence of the Mo^{5+} and/or Mo^{6+} cation in the MoO_x film, as well as to increase the work function.

3.4. MoO_x as a buffer layer between p-a-Si:H/ITO interface

In this section, the above-mentioned MoO_x films were applied into SHJ solar cells to study their influence on device performance. In the first step, the MoO_x film was inserted as a buffer layer between TCO and p-type a-Si:H emitting layer in a conventional SHJ cell. As can be seen from Fig. 6(a), the conversion efficiency of the reference SHJ solar cell is 18% with V_{oc} of 715.9 mV, J_{sc} of 38.33 mA/cm^2 and FF of 65.58%. On the contrary, the insertion of 5 nm MoO_x between TCO and a-Si:H(p) can effectively increase V_{oc} up to 719.6 mV and FF up to 70.24%, respectively. However, the J_{sc} slightly decreased to 37.75 mA/cm^2, which can be contributed to the parasitic absorption of MoO_x because of its relatively low optical transmittance. It can be seen from Fig. 6(b) that although these two solar cells behave very similar to EQE spectral responses in the infrared band, the EQE spectral response in the visible region of the reference SHJ solar cell is obviously higher than that of the device with MoO_x buffer layer. Finally, the conversion efficiency was improved to 19.1%, which can be attributed to the decrease of contact barrier and improvement of energy level matching between TCO and a-Si:H(p) interface by inserting the MoO_x buffer layer.

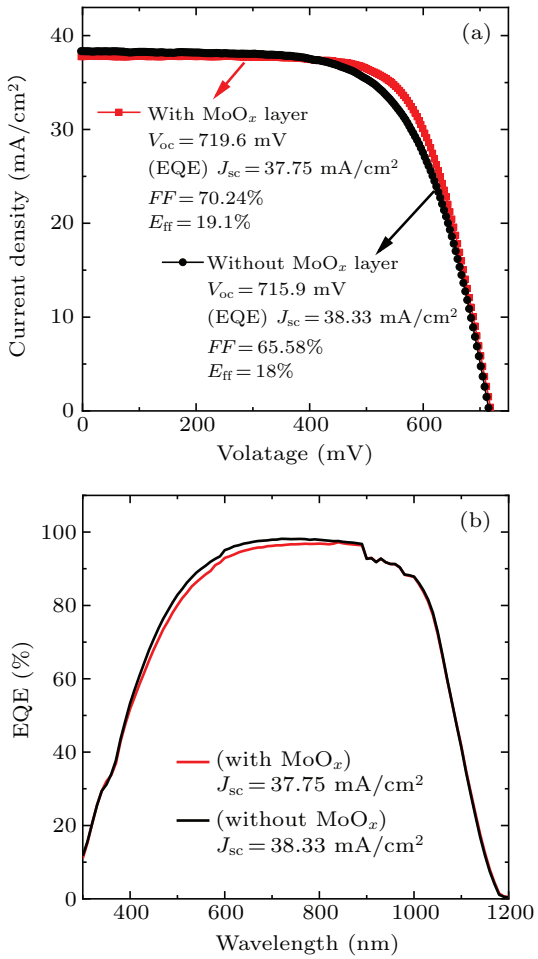


Fig. 6. Comparison of conventional SHJ solar cells with or without sputtered 5 nm MoO_x buffer layer with (a) J–V curves, (b) EQE spectra.

3.5. MoO_x as the hole selective transport layer

In the following step, the MoO_x film as a hole selective transport layer was applied into a SHJ solar cell to replace

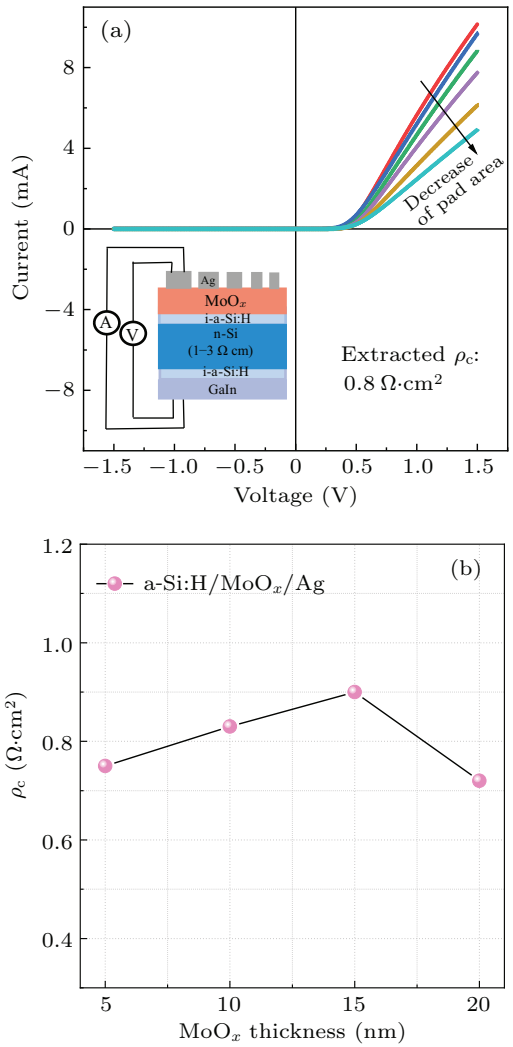


Fig. 7. Contact resistivity ρ_c measurements of MoO_x-based contacts to n-type c-Si. (a) A series of I–V measurements of the samples with optimal thickness of MoO_x films, and (b) the ρ_c with different thickness. Schematics of the contact resistivity test structure samples is included in inset.

the a-Si:H(p) emitting layer. To evaluate the hole-selective contact behavior of the i-a-Si:H/MoO_x, the contact resistivity ρ_c was measured by using the method devised by Cox and Strack. A series of current–voltage (I–V) measurements of the samples with optimal thickness of MoO_x films and the ρ_c with different thickness are presented in Fig. 7, with the test structure in the inset. As can be seen in Fig. 7(a), the sample with Ag directly deposited MoO_x exhibited Schottky contacts for different sizes area pads. We determined the extracted contact resistivity ρ_c for the structure with n-Si/a-Si:H/MoO_x/Ag to be 0.8 $\Omega\cdot cm^2$.

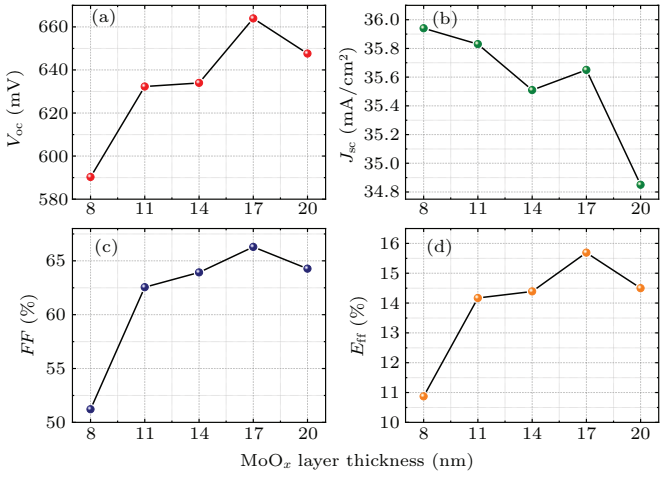


Fig. 8. The influence of MoO_x thickness on J–V output parameters (a) V_{oc}, (b) J_{sc}, (c) FF and (d) E_{ff}.

The influence of MoO_x thickness on J–V parameters of SHJ solar cells with MoO_x as the hole selective layers are shown in Fig. 8. In fact, the increase of MoO_x thickness has two opposite effects: the positive one is to improve the passivating quality and built-in electric field because of fully covered c-Si surface by thick enough MoO_x layer, while the negative one is to increase the series resistance and parasitic absorption. The increase of series resistance would hinder the carrier transport and then lead to V_{oc} and FF decrease, while the increase of parasitic absorption will result in J_{sc} decrease. The results in Fig. 8 indicate that with the increase of MoO_x thickness the J_{sc} monotonically decrease. On the contrary, the V_{oc} and FF demonstrate peak values when the MoO_x thickness is 17 nm, which can be contributed by balancing the above-mentioned positive and negative effects. Eventually, a 17 nm MoO_x film prepared by sputtering method is successfully used as the hole transport layer in SHJ solar cell, and the conversion efficiency reach the maximum value of 15.69%. Based on the above results, the MoO_x films with sufficient thickness are able to obtain good passivating quality and build a high built-in electric field to achieve carrier selectivity. In order to further improve the passivation effect, we try to increase the thickness of the a-Si:H(i) passivation layer and reduce the deposition temperature of thermal evaporated ITO films. Although the thicker a-Si:H layer limiting the short-circuit current density, the V_{oc} and FF are significantly improved. Finally, a champion conversion efficiency of 17.5% with V_{oc} of 711 mV, J_{sc} of 32.8 mA/cm^2 and FF of 74.9% is currently obtained, as shown in Fig. 9. As mentioned above, a relatively thick (17 nm) MoO_x film results in a decrease of J_{sc}. This is consistent with the optical results, where 17-nm-thick MoO_x film demonstrated the poor optical transmittance around 75% (the red curve) in the visible spectrum region, as shown in Fig. 10. We infer that the lower transmittance may be related to the ion bombardment on MoO_x films and deteriorate the film quality during the sputtering process. Further optimization will be carried out including pre-treatment, post-annealing in various gaseous environments, mesh electrode with bias voltage, etc. to control the ion damage on the films and interfaces and then ultimately improve the device performance. Moreover, oxygen vacancies in TMOs appear during film deposition or exposure to air.[28] According to the UPS test results, the factors affecting the work function of the oxygen concentration in the metal oxide should be taken into consideration. The main factors that reduce the device performance with the sputtered MoO_x film require further intensive research.

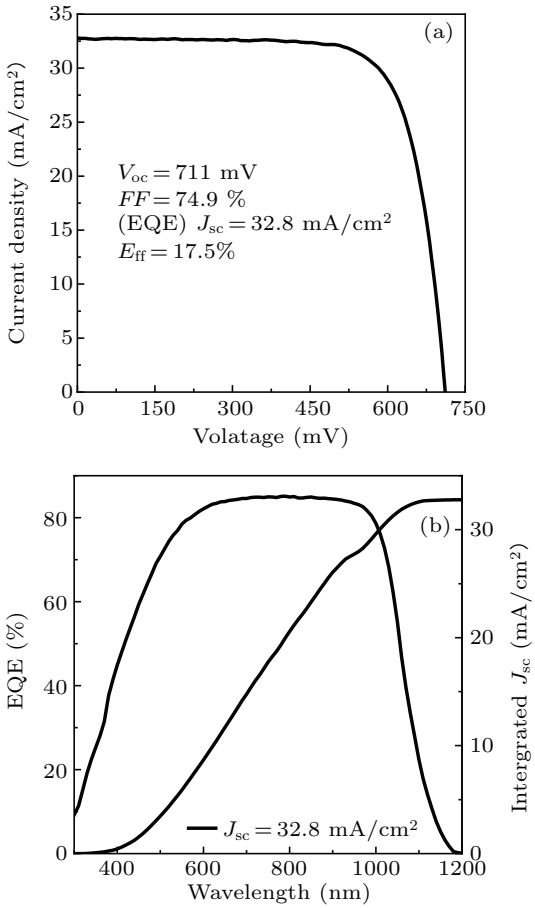


Fig. 9. The champion SHJ solar cell with 17 nm MoO_x hole transport layer: (a) J–V curve, (b) EQE spectra.

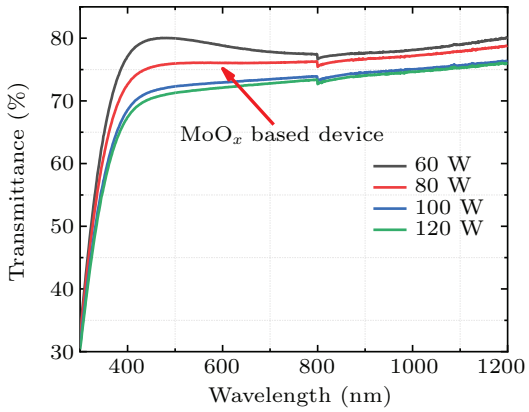


Fig. 10. The transmittance of MoO_x films prepared under various RF sputtering power.

4. Conclusion

The effects of MoO_x as buffer layer and hole transport layer on the performance of SHJ solar cells were investigated. The results show that the high work function of MoO_x layer enable to significantly improve the performance of solar cells. By inserting a 5 nm MoO_x buffer layer between a-Si:H(p)/ITO interface result in an efficiency of 19.1% with V_{oc} of 719.6 mV, J_{sc} of 37.75 mA/cm^2, and *FF* of 70.24%. In addition, the best conversion efficiency of 17.5% and *FF* of 74.9% were obtained by using 17 nm MoO_x film as the hole selective layer to replace the p-type a-Si:H emitting layer. These results in this manuscript confirm the feasibility of a sputtering process of MoO_x films and their application in SHJ solar cells. Further optimization of magnetron sputtered MoO_x is urgently deserved to improve SHJ solar cell performance.

Acknowledgements

Project supported by the National Natural Science Foundation of China (Grant No. 62074084), the National Key Research and Development Program of China (Grant No. 2018YFB1500402), and Key Research and Development Program of Hebei Province, China (Grant No. 20314303D).

References

[1] Louwen A, Sark W V, Schropp R and Faaij A 2016 *Sol. Energy Mater. Sol. Cells* **147** 295
[2] Cotter J E, Guo J H, Cousins P J, Abbott M D, Chen F W and Fisher K C 2006 *IEEE Trans. Electron Devices* **53** 1893
[3] Yoshikawa K, Yoshida W, Irie T, Kawasaki H, Konishi K, Ishibashi H, Asatani T, Adachi D, Kanematsu M, Uzu H and Yamamoto K 2017 *Sol. Energy Mater. Sol. Cells* **173** 37
[4] Richter A, Smirnov V, Lambertz A, Nomoto K, Welter K and Ding K N 2018 *Sol. Energy Mater. Sol. Cells* **174** 196
[5] Zhou J K, Zhang B Y, Chen J F, Ren H Z, Huang Q, Zhang X D, Hou G F and Zhao Y 2021 *Appl. Phys. A* **127** 735
[6] Nogay G, Seif J P, Riesen Y, Tomasi A, Jeangros Q, Wyrsch N, Haug F J, Wolf S D and Ballif C 2016 *IEEE J. Photovolt* **6** 1654
[7] Bivour M, Temmler J, Steinkemper H and Hermle M 2015 *Sol. Energy Mater. Sol. Cells* **142** 34
[8] Greiner M T, Helander M G, Tang W M, Wang Z B, Qiu J and Lu Z H 2011 *Nat. Mater.* **11** 76
[9] Meyer J, Hamwi S, Kroger M, Kowalsky W, Riedl T and Kahn A 2012 *Adv. Mater.* **24** 5408
[10] Oh W K, Hussain S Q, Lee Y J, Lee Y, Ahn S and Yi J 2012 *Mater. Res. Bull.* **47** 3032
[11] Park Y S, Kim E, Hong B and Lee J 2013 *Mater. Res. Bull.* **48** 5115
[12] Kim M, Kim J, Cho J, Kim H, Lee N and Choi B 2016 *Mater. Res. Bull.* **82** 115
[13] Ghahfarokhi O M, Chakanga K, Geissendoerfer S, Sergeev O, Maydell K and Agert C 2015 *Prog. Photovolt: Res. Appl.* **23** 1340
[14] Kim S, Jung J, Lee Y J, Ahn S, Hussain S Q, Park J, Song B S, Han S, Dao V A, Lee J and Yi J 2014 *Mater. Res. Bull.* **58** 83
[15] Almora O, Gerling L G, Voz C, Alcubilla R, Puigdollers J and Garcia-Belmonte G 2017 *Sol. Energy Mater. Sol. Cells* **168** 221
[16] Masmitjà G, Ortega P, Puigdollers J, L. Gerling G, Martín I, Voz C and Alcubilla R 2018 *J. Mater. Chem. A* **6** 3977
[17] Zheng S Z, Li W L, Su T T, Xie F Y, Chen J, Yang Z Y, Zhang Y, Liu S W, Aldred M P, Wong K Y, Xu J R and Chi Z G 2018 *Sol. RRL* **2** 1700245
[18] Xu Z Y, Peng S L, Lin H, Tian S H, Wang Z L, He J, Cai L, Hou J and Gao P Q 2021 *Sol. RRL* **5** 2100064
[19] Essig S, Dréon J, Rucavado E, Mews M, Koida T, Boccard M, Werner J, Geissbühler J, Löper P, Morales-Masis M, Korte L, Wolf S D and Ballif C 2018 *Sol. RRL* **2** 1700227
[20] Battaglia C, Nicolás S M, Wolf S, Yin X T, Zheng M, Ballif C and Javey A 2014 *Appl. Phys. Lett.* **104** 113902
[21] Hussain S Q, Mallem K, Kim Y J, Tuan Le A H, Khokhar M Q, Kim S, Dutta S, Sanyal S, Kim Y, Park J, Lee Y, Cho Y H, Cho E C and Yi J 2019 *Mater. Sci. Semicond. Process.* **91** 267
[22] Bullock J, Wan Y M, Xu Z R, Essig S, Hettick M, Wang H C, Ji W B, Boccard M, Cuevas A, Ballif C and Javey A 2018 *ACS Energy Lett.* **3** 508
[23] Shi J H, Shen L L, Liu Y W, Yu J, Liu J N, Zhang L P, Liu Y C, Bian J Y, Liu Z X and Meng F Y 2018 *Mater. Res. Bull.* **97** 176
[24] Shrotriya V, Li G, Yao Y, Chu C W and Yang Y 2006 *Appl. Phys. Lett.* **88** 073508
[25] Bullock J, Hettick M, Geissbühler J, Ong A J, Allen T, Sutter-Fella C M, Chen T, Ota H, Schaler E W, Wolf S D, Ballif C, Cuevas A and Javey A 2016 *Nature Energy* 15031
[26] Klein A, Korber C, Wachau A, Sauberlich F, Gassenbauer Y, Harvey S P, Proffit D E and Mason T O 2010 *Materials (Basel)* **3** 4892
[27] Wan Y M, Karuturi S K, Samundsett C, Bullock J, Hettick M, Yan D, Peng J, Narangari P R, Mokkapati S, Tan H H, Jagadish C, Javey A and Cuevas A 2017 *ACS Energy Lett.* **3** 125
[28] Greiner M T and Lu Z H 2013 *NPG Asia Mater.* **5** e55
[29] Sian T S and Reddy G B 2005 *J. Appl. Phys.* **98** 026104
[30] Sabhapathi V K, Hussain O M, Uthanna S, Naidu B S, Reddy P J, Julien C and Balkanski M 1995 *Mater. Sci. Eng. B* **32** 93
[31] Ramana C V and Julien C M 2006 *Chem. Phys. Lett.* **428** 114
[32] Uthanna S, Nirupama V and Pierson J F 2010 *Appl. Surf. Sci.* **256** 3133
[33] SrinivasaRao K, Kanth B R and Mukhopadhyay P K 2009 *Appl. Phys. A* **96** 985
[34] Navas I, Vinodkumar R, Lethy K J, Detty A P, Ganesan V, Sathe V and Mahadevan Pillai V P 2009 *J. Phys. D* **42** 175305
[35] Mohamed S H and Venkataraj S 2007 *Vacuum* **81** 636
[36] Dhanasankar M, Purushothaman K K and Muralidharan G 2011 *Appl. Surf. Sci.* **257** 2074
[37] Boccard M, Ding L, Koswatta P, Bertoni M and Holman Z 2015 *IEEE 42nd Photovoltaic Specialist Conference (PVSC)*
[38] Bivour M, Zähringer F, Ndione P and Hermle M 2017 *Energy Procedia* **124** 400
[39] Dréon J, Jeangros Q, Cattin J, Haschke J, Antognini L, Ballif C and Boccard M 2020 *Nano Energy* **70** 104495